Journal of Quantitative Spectroscopy & Radiative Transfer 277 (2022) 107985

Contents lists available at ScienceDirect

Journal of Quantitative Spectroscopy & Radiative Transfer

journal homepage: www.elsevier.com/locate/jqsrt

Laser-induced frequency shift in a spin-1 Bose–Einstein condensate of sodium

Ningxuan Zheng[a], Wenliang Liu[a,b], Vladimir Sovkov[a,c], Li Tian[a], Yuqing Li[a,b], Yongming Fu[a], Peng Li[a], Jizhou Wu[a,b,*], Jie Ma[a,b,**], Liantuan Xiao[a,b], Suotang Jia[a,b]

[a] State Key Laboratory of Quantum Optics and Quantum Optics Devices, Institute of Laser Spectroscopy, Shanxi University, Taiyuan 030006, China
[b] Collaborative Innovation Center of Extreme Optics, Shanxi University, Taiyuan 030006, China
[c] St. Petersburg State University, 7/9 Universitetskaya nab., St. Petersburg 199034, Russia

ARTICLE INFO

Article history:
Received 1 July 2021
Revised 27 September 2021
Accepted 21 October 2021
Available online 27 October 2021

Keywords:
Laser-induced frequency shift
Photoassociation
Spinor Bose–Einstein condensate

ABSTRACT

Experimental measurement and analysis of the laser-induced frequency shifts (LIFSs) of photoassociation (PA) spectra in a spinor Bose–Einstein condensate (BEC) of sodium is reported. The trap loss spectra of the atoms in the BEC were recorded at different PA laser intensities. Linear variations of the frequency shift for different spin components were demonstrated. The analogous linear dependence on the intensity of the full width at half maximum (FWHM) of the spectra was also shown. The slopes of the linear relationships of the shift and broadening are both independent of spin component within the error range of the experiment. A theoretical model, considering the interactions of three channels (a scattering continuum state, a single bound level near the scattering state, and an optically excited light-dressed level), explains the linear dependence of the LIFSs and the FWHM broadening on the PA laser power. The experimental results are consistent with the theoretical calculations.

1. Introduction

Understanding collisional properties of atoms and molecules at ultracold temperatures has been a long-term goal in quantum simulation and chemical physics due to the importance of the scattering resonances [1]. Bose–Einstein condensates (BECs) of ultracold neutral atomic gases, as a collective quantum system, have served as ideal platforms to investigating the fundamental physical problems (including the scattering problems) since their first experimental realizations in 1995 [2,3]. Spinor BECs, whose Zeeman or hyperfine substates are often coherently coupled via two photon Raman transitions, have recently drawn considerable attention from both theory and experiment [4–6]. In addition, research into spinor BECs has proven that the $F = 1$ and $F = 2$ hyperfine spin states of ^{87}Rb atoms [7–12] and the $F = 1$ hyperfine spin manifolds of ^{23}Na atoms [13–16] are ideal candidate systems to investigate the spinor dynamics induced by the interplay of the spin-dependent interaction, the quadratic Zeeman energy for a spin-1 condensate [14,15,17,18] and a spin-2 condensate [10,12]. By controlling the spin degrees of freedom, a spinor BEC has become an excellent quantum simulator [7,8].

Photoassociation (PA) of ultracold atoms in a BEC has been used to produce ultracold molecules and to tune the atomic scattering length [19,20]. Photoassociation spectroscopy (PAS) is employed to determine interatomic interaction potentials with ultrahigh precisions . A PA process can also control spin-dependent interactions and is beneficial for increasing the strength of the ferromagnetic interaction in spinor BECs [21]. Nonetheless, many gaps in our knowledge still need to be filled in the research of PA in spinor BECs.

BECs provide ideal platforms in which to perform accurate measurements of PA line positions of atomic or molecular transitions as well as of laser-induced frequency shifts (LIFSs) [22]. LIFSs of rovibrational levels of ultracold molecules are caused by the energy coupling between the atom-atom scattering state and a molecular bound state. This coupling must be understood when manipulating ultracold molecular states and controlling inter-atomic interactions [23,24].

Experimentally, LIFSs have been widely investigated in homonuclear gases of ^{7}Li [22,25,26], ^{23}Na [1], ^{87}Rb [27], ^{133}Cs [28,29], and a mixture of ^{23}Na and ^{133}Cs atomic gases [30]. The LIFSs are essential in the production of ultracold molecules in a specific state [31], the manipulation of molecular quantum states [24], and precise measurements of the s-wave scattering

* Corresponding author at: State Key Laboratory of Quantum Optics and Quantum Optics Devices, Institute of Laser Spectroscopy, Shanxi University, 92 Wucheng Road, Taiyuan 030006, China
** Co-corresponding author.
E-mail addresses: wujz@sxu.edu.cn (J. Wu), mj@sxu.edu.cn (J. Ma).

https://doi.org/10.1016/j.jqsrt.2021.107985
0022-4073/

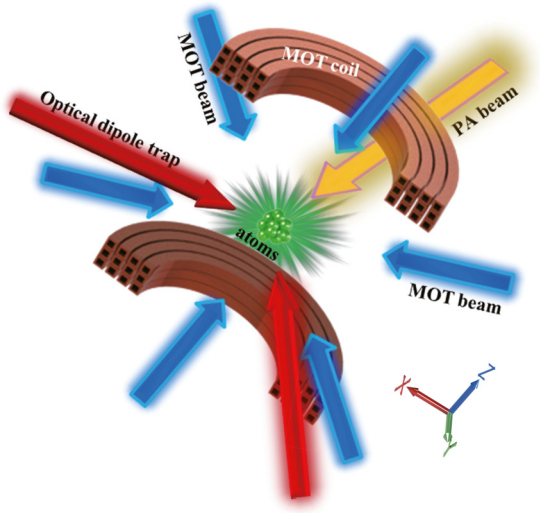

Fig. 1. A schematic diagram of the experiment. The MOT is constructed with six MOT beams (blue arrows) from three orthogonal directions and a pair of anti-Helmholtz MOT coils. The crossed optical dipole trap (red arrows) is used for the realization of the spinor BECs (green ensemble). The yellow arrow represents the PA laser beam. (For interpretation of the references to color in this figure legend, the reader is referred to the web version of this article.)

length [32]. However, LIFSs in spinor BECs, especially for the $m_F = 0, \pm 1$ spin components, have yet to be explored. A variation of LIFSs for different m_F components reflects different values for scattering lengths.

In the present paper, we demonstrate PAS in a sodium spinor condensate. The PA transition to the $v = 4, J = 2$ rovibrational level of the 0_g^- pure long-range state is investigated for several PA laser intensities. The experiments showed a red shift for the LIFSs of the transition and a broadening of the full width at half maximum (FWHM). The LIFSs and the FWHM broadening for different spin components exhibited a linear behavior with PA intensity for the range of intensities used in our experiment. A theoretical model considering the interactions of three channels (a scattering continuum, a single bound level near the scattering state, and an optically excited light-dressed level) is established. The experimental results are consistent with the theoretical calculations.

2. Experimental setup

The experimental setup has three parts: the oven chamber, the Zeeman slower, and the science chamber. The oven contains 25 g of solid sodium heated to 532 K. At this temperature sodium has a vapor pressure of 2.3×10^{-5} Pa. A zero-crossing Zeeman slower is used to slow down the atoms ejected from a pin hole in the oven [33]. The science chamber is at the end of the Zeeman slower, in which laser and evaporation cooling as well as the PA experiments on spinor condensates are carried out. The chamber has two re-entrant viewports, one each at the top and bottom as well as eight viewports in the horizontal plane for the access of laser beams for cooling, dipole trapping, imaging, and PA. An ion pump (Agilent Star Cell, 150 L/s) and a Ti-sublimation pump are used to keep the pressure in the science chamber at 1.5×10^{-11} Torr.

Atoms are collected and cooled in a magneto-optical trap (MOT) [34], as shown in Fig. 1. The MOT beams (trapping, repumping) are provided by a TA-SHG laser system (589 nm, Toptica). After 8 s of MOT loading, about 5×10^9 atoms with a temperature of 350 μK are trapped. In order to further lower the temperature, we transition into a compressed magneto-optical trap (CMOT) and use optical molasses cooling [35]. We reach 45 μK with 4×10^8 atoms. To de-pump atoms into the $F = 1$ hyperfine state, repumping beams are extinguished 1 ms before the MOT beams and coils are switched off.

The precooled sodium atoms are then loaded into a crossed optical dipole trap (CODT) generated by two horizontally crossed laser beams, one in the X and one in the Y direction. The beams are focused to a $1/e^2$ beam diameter of 32 μm (35 μm) and have a power of 13 W (14 W) in the X (Y) direction, respectively. After 400 ms loading, about 7×10^6 atoms with a temperature of 70 μK are trapped. Forced evaporation cooling is immediately performed by reducing the power in the dipole trap lasers. The trapping potential that the atoms experience is exponentially reduced within 3 s and we obtain a spinor BEC with 2×10^5 atoms in the $F = 1$ ground state and a phase space density (PSD) of 7.6. (The three m_F states have equal population as confirmed with the Stern-Gerlach method.) In the CODT, the trapping frequencies near the bottom of the potential well are $(\omega_X, \omega_Y, \omega_Z) = 2\pi \times (314 \pm 2.8, 306 \pm 3.0, 367 \pm 3.2$ Hz). Then for up to a few milliseconds a PA beam interacts with the spinor BEC. The size of the BEC along the PA beam direction, measured by magnified absorption imaging, is 21 μm, which is smaller than the $1/e^2$ beam diameter of the PA beam of 108 μm. An acousto-optic modulator (Gooch & Housego 3080-125) is used to control the PA beam power and PA pulse duration with a rise time of 60 ns, which is orders of magnitude less than the PA pulse duration. The peak intensity of the PA beam can be adjusted between 23 and 1390 W cm^{-2}. The polarization of PA beam is linear and parallel to the Z axis. An external bias magnetic field of about 200 mG is applied along this same Z axis. The projection quantum number m_F of the atoms are defined relative to this external magnetic field.

The frequency of the PA laser is tuned near the $v = 4, J = 2$ molecular rovibrational level of the Na_2 0_g^- pure long-range state below the $3S_{1/2} + 3P_{3/2}$ dissociation limit. When the frequency is tuned to the resonance position, PA leads to loss of atoms as excited molecules can spontaneously decay into ground-state molecules or pairs of hot atoms escaping the trap. The frequency of the PA laser is locked using a wavelength meter feedback system and the frequency stability is 5 MHz. The PA laser makes 6 MHz steps along the relevant frequency range and three measurements are taken for each lock. The average of the number of measured atoms in the three experiments is counted. Then they are normalized by the number of remaining atoms after a far detuned PA illumination. Absorption imaging of the condensates for each experiment was performed 5 ms after the PA laser and the dipole traps were turned off.

In our experiment, PA spectra are acquired through atom loss as a function of PA frequency. Fig. 2 shows a series of typical trap loss PA spectra shifting with PA laser intensity for the unpolarized $F = 1$ state. The maximum loss of the number of atoms occurs at the resonance position. The FWHM of the spectral line is defined by the Lorentz fitting curve. The increase of the PA laser intensity leads to broadening of the FWHM and a red shift of the resonance position. The red shift of the resonance position as the PA laser intensity increases is namely, the LIFSs.

The dependence of the maximum atom loss ratio in the PA spectra on the PA pulse duration at different power intensities is measured. We found no obvious relation between the resonance position and duration of the PA lines. Fig. 3 shows the saturation of the maximum atom loss ratio as a function of PA pulse duration at an intensity of 354 W cm^{-2}.

According to the duration that leads to the saturation of the maximum atom loss ratio at different PA laser intensities, a fluence (intensity × pulse duration) of the PA laser pulse is fixed at 276 ms W cm^{-2}. The value is determined based on two factors. Firstly, the pulse duration should be saturated. Secondly, the PA pulse duration of high-power should be small enough to avoid the severe heating of the atoms that leading to the inaccurate mea-

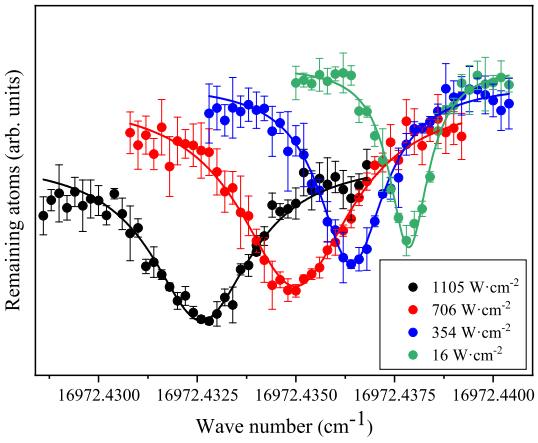

Fig. 2. PA spectra of the $v = 4$, $J = 2$ rovibrational level of the Na_2 0_g^- pure long-range state for $F = 1$ spinor sample at four PA laser intensities: $I_{PA} = 16$ W cm^{-2} (green balls), 354 W cm^{-2} (blue balls), 706 W cm^{-2} (red balls), and 1105 W cm^{-2} (black balls), respectively. The fluence is the same for the four spectra. The resonance peaks are fitted to Lorentzians (solid curves). (For interpretation of the references to color in this figure legend, the reader is referred to the web version of this article.)

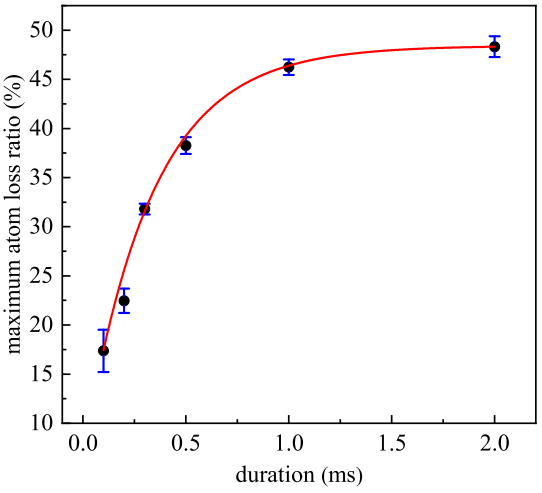

Fig. 3. The dependence of maximum loss from the $F = 1$ spinor condensate with all m_F levels equally populated on the duration of PA pulse at an intensity of 354 W cm^{-2}.

surement. Actually, the pulse duration determined by the fixed fluence is optimized between 12,000-200 μs corresponds to a peak intensity from 23 to 1390 W cm^{-2}.

3. Experimental results

To explore the influence of different spin states on the LIFSs, we manipulate the gradient magnetic field generated by the MOT coils and apply radio frequency radiation to prepare different spin components. For a pure $m_F = -1$ atomic sample, we apply a 10 G/cm gradient field for 1 s at the start of the forced evaporation in the CODT [36]. For a pure $m_F = 0$ sample we apply a 20 G/cm gradient field within 1 s before the end of the forced evaporation in the CODT [37]. For a pure $m_F = +1$ sample, the atoms are first prepared in the $m_F = -1$ state and then transferred to the $m_F = +1$ state with radio frequency radiation.

Fig. 4 shows the spectral FWHM as a function of the PA laser intensity for different spin states at our fixed fluence of 276 ms W cm^{-2}. Some FWHM at PA intensities above 1.2 kW cm^{-2} are unreliable and not shown, because the corresponding short pulse length makes the PAS unsaturated. The FWHM and intensity are linearly related. The slopes are the same within our error range.

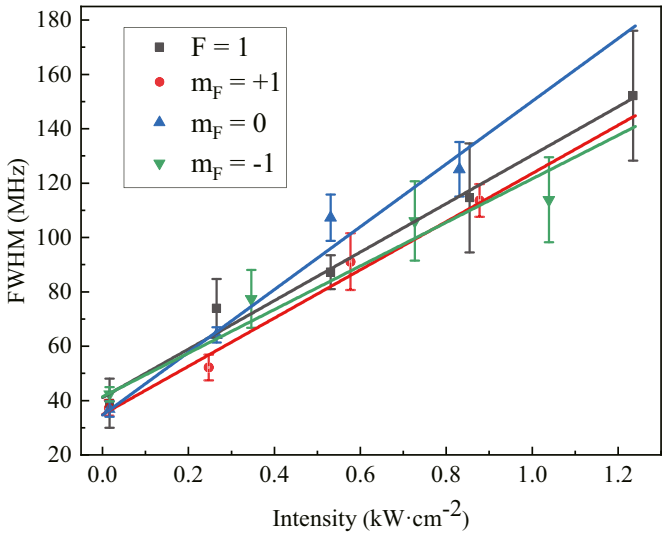

Fig. 4. FWHM with one-standard-deviation uncertainties as functions of PA laser intensity for the unpolarized $F = 1$ state (black squares), $m_F = +1$ state (red dots), $m_F = 0$ state (blue triangles), and $m_F = -1$ state (green triangles). The colored solid lines represent linear fits to the corresponding experimental data. (For interpretation of the references to color in this figure legend, the reader is referred to the web version of this article.)

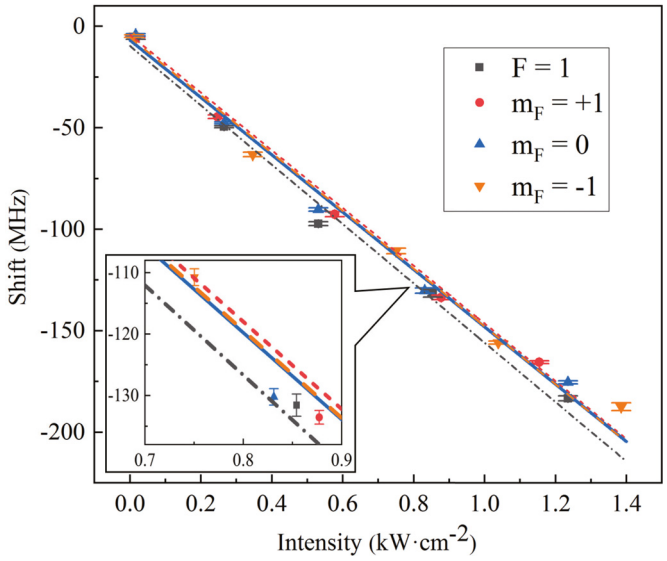

Fig. 5. The spectral shift with one-standard-deviation uncertainties as a function of PA laser intensity for the unpolarized $F = 1$ (black squares), $m_F = +1$ (red dots), $m_F = 0$ (blue triangles), and $m_F = -1$ (orange triangles) states. The colored dashed and solid lines represent linear fits to the experimental data. The differences between the data and fits near $I_{PA} = 0.8$ kW cm^{-2} are shown in the inset. (For interpretation of the references to color in this figure legend, the reader is referred to the web version of this article.)

In Fig. 5, the spectral shift as a function of the PA laser intensity for different spin states is shown. The linear slopes of different spin components are the same within the error range. Experimental errors in this figure as well as in Fig. 4 are mainly attributed to fitting errors, systematic uncertainties induced by particle number fluctuation in each experiment, and small uncertainties in measuring the intensity of the PA laser.

The measured FWHM broadening slopes and LIFSs slopes are also shown in Table 1.

Table 1
The measured FWHM broadening and LIFSs slopes with their one-standard deviation uncertainties. All quantities are in MHz/(kW cm^{-2}) .

	This work (0_g^- for Na_2)		Previous work ($A_1\Sigma_u^+$ for Na_2 [1])
Spin state	FWHM broadening	LIFSs	LIFSs
$F = 1$	89.21 ± 8.65	-146.17 ± 9.10	
$m_F = +1$	88.69 ± 6.12	-142.20 ± 3.80	
$m_F = 0$	115.48 ± 10.62	-141.27 ± 7.29	
$m_F = -1$	80.16 ± 9.65	-142.39 ± 5.98	-164 ± 35

4. Theoretical analyses

The linear dependence of the spectral shift on the laser intensity is consistent with the theoretical predictions [22,23]. Recent modeling [38] devoted to PA LIFSs in cesium used a three-channel model, analyzed using Green's functions [39,40]. Our work employs the same model, however, we re-derived all equations using a projection technique similar to that used by Feshbach [41–43].

Briefly, the three channels comprise of a continuum of scattering states P, a single bound level Q, and an optically excited light-dressed level R, with the zero-th order (unperturbed) energies ϵ_P, ϵ_Q, and ϵ_R respectively. The scattering states lie above the threshold (dissociation limit) with the conventionally zero energy, $\epsilon_P > 0$. The projectors $\mathbf{P}_P$, $\mathbf{P}_Q$, and $\mathbf{P}_R$ are applied to the Hamiltonian $\mathbf{H}$ to find a system of coupled equations for the projections (partial amplitudes) of the full (mixed) eigenstate $|E\rangle$ onto the uncoupled basis functions $|\epsilon_P\rangle$, $|\epsilon_Q\rangle$, and $|\epsilon_R\rangle$:

$$\langle\epsilon_P|E\rangle = \delta(E-\epsilon_P) + \frac{1}{E^+-\epsilon_P}[W_{PQ}(\epsilon_P)\langle\epsilon_Q|E\rangle + W_{PR}(\epsilon_P)\langle\epsilon_R|E\rangle], \tag{1}$$

$$[E-\epsilon_Q]\langle\epsilon_Q|E\rangle = W_{QP}(E) + W_{QR}\langle\epsilon_R|E\rangle \tag{2}$$

$$+\int_0^\infty \frac{W_{QP}(\epsilon_P)W_{PQ}(\epsilon_P)}{E^+-\epsilon_P}\,d\epsilon_P\langle\epsilon_Q|E\rangle + \int_0^\infty \frac{W_{QP}(\epsilon_P)W_{PR}(\epsilon_P)}{E^+-\epsilon_P}\,d\epsilon_P\langle\epsilon_R|E\rangle,$$

$$[E-\epsilon_R]\langle\epsilon_R|E\rangle = W_{RP}(E) + W_{RQ}\langle\epsilon_Q|E\rangle \tag{3}$$

$$+\int_0^\infty \frac{W_{RP}(\epsilon_P)W_{PR}(\epsilon_P)}{E^+-\epsilon_P}\,d\epsilon_P\langle\epsilon_R|E\rangle + \int_0^\infty \frac{W_{RP}(\epsilon_P)W_{PQ}(\epsilon_P)}{E^+-\epsilon_P}\,d\epsilon_P\langle\epsilon_Q|E\rangle$$

with $E^+ = E + \mathrm{i}0$, $W_{PQ}(\epsilon_P) = W^*_{QP}(\epsilon_P) \equiv \langle\epsilon_P|\mathbf{H}|\epsilon_Q\rangle$, $W_{RP}(\epsilon_P) = W^*_{PR}(\epsilon_P) \equiv \langle\epsilon_R|\mathbf{H}|\epsilon_P\rangle$, $W_{QR} = W^*_{RQ} \equiv \langle\epsilon_Q|\mathbf{H}|\epsilon_R\rangle$. As argument of the functions W_{ab}, we only show the scattering state energies, when essential for the formulae. In our simplified theory, we considered a fixed small scattering energy E: the spread of energies is very narrow in a BEC.

After some tiresome algebra, the solution is found, producing the following results. The transition probability $\rho(E,\delta) = |\langle\epsilon_R|E\rangle|^2$ to the excited state, R, as a function of the initial energy E and the transition energy shift δ (with the observed transition energy $\hbar\omega = \epsilon_R - E + \delta$) is given as

$$\rho(E,\delta) = \frac{w(E)}{\pi}\frac{1}{(\delta-\delta_m(E))^2 + w(E)^2}. \tag{4}$$

The first factor of Eq. 4 does not depend on the shift δ and reproduces the famous result by Fano [44,45] for the transition probability from the two-channel coupled state $P \sim Q$ with energy E to the unperturbed upper state R (the weak intensity approximation) as follows:

$$\frac{w(E)}{\pi} = |W_{PR}(E)|^2\left[\frac{(\beta+q)^2}{\beta^2+1}\right], \tag{5}$$

where $W_{PR}(E)$ is the electric transition dipole moment, from the uncoupled scattering state with the energy $\epsilon_P = E$ to the photoassociated state,

$$\beta = \frac{E-\epsilon_Q-F_{QQ}(E)}{\pi|W_{PQ}(E)|^2}$$

is the reduced initial state energy,

$$q = \frac{W_{RQ}+F_{QR}(E)}{\pi W_{QP}(E)W_{RP}(E)}$$

is the Fano asymmetry parameter, and

$$F_{AB}(E) = \mathcal{P}\int \frac{W_{AP}(\epsilon_P)W_{PB}(\epsilon_P)}{E-\epsilon_P}\,d\epsilon_P$$

with $\mathcal{P}$ representing the principal value of the integral.

The second factor of Eq. (4) is a Lorentzian as a function of δ for fixed E, which validates the use of the Lorentzian function for the fit of the observed PA line profiles in a Bose–Einstein condensate (Fig. 2). The maximum of the Lorentzian is located at

$$\delta_m(E) = \pi|W_{PR}(E)|^2\left[\frac{(q^2-1)\beta-2q}{\beta^2+1}\right] - F_{RR}(E). \tag{6}$$

The quantities q and β deal with the coupled lower state and not with the PA transition and are independent of the PA laser intensity I_{PA}. The electric–dipole transition amplitude W_{PR} is a linear function of the electric field $\mathcal{E} \sim \sqrt{I_{PA}}$. This fact, with Eqs. (5) and (6), shows that the position δ_m of the profile maximum and the FWHM $2w$, are linear functions of the PA laser intensity I_{PA}, at least within the adopted model.

The parameters of the profile Eqs. (5) and (6) depend on the energy ϵ_Q of the near-dissociation bound level, i.e., implicitly on the scattering length (e. g., [21]). Such change was not detected for different m_F in our experiment.

5. Conclusions

In summary, we have presented measurements of the LIFSs and the FWHM for the PA of the $v = 4$, $J = 2$ molecular rovibrational level of the Na_2 0_g^- pure long-range state in a sodium spinor BEC. Results show that the shift and the FWHM broadening are linearly dependent on PA laser intensity, which agrees well with a theoretical model with three coupled channels. The same slopes for the three different spin components imply that the closest to the first dissociation limit bound-state energies and the scattering lengths are similar. The methods and results provide deep insights into the scattering mechanism for the creation of ground state molecules in a spinor condensate. Our work could be generalized to spinor condensates of other species.

Declaration of Competing Interest

The authors declared that they have no conflicts of interest to this work.

We declare that we do not have any commercial or associative interest that represents a conflict of interest in connection with the work submitted.

Acknowledgments

This work is supported by the National Natural Science Foundation of China (Grants nos. 61901249, 62020106014), the National Key R&D Program of China (Grant no. 2017YFA0304203), PCSIRT (No. IRT-17R70), 111 project (Grant no. D18001), the Program for the Outstanding Innovative Teams of Higher Learning Institutions of Shanxi (OIT), the Applied Basic Research Project of Shanxi Province, China (Grant nos.201901D211191, 201901D211188) and the collaborative grant by the Russian Foundation for Basic Research and NSF of China (62011530047, and No. 20-53-53025 in the RFBR classification).

References

[1] McKenzie C, Hecker Denschlag J, Häffner H, Browaeys A, de Araujo LEE, Fatemi FK, et al. Photoassociation of sodium in a Bose–Einstein condensate. Phys Rev Lett 2002;88:120403. doi:10.1103/PhysRevLett.88.120403.
[2] Anderson MH, Ensher JR, Matthews MR, Wieman CE, Cornell EA. Observation of Bose–Einstein condensation in a dilute atomic vapor. Science 1995;269(5221):198–201.
[3] Davis KB, Mewes M-O, Andrews MR, van Druten NJ, Durfee DS, Kurn D, et al. Bose–Einstein condensation in a gas of sodium atoms. Phys Rev Lett 1995;75(22):3969.
[4] Zhai H. Degenerate quantum gases with spin–orbit coupling: a review. Rep Prog Phys 2015;78(2):026001.
[5] Wang P, Yu Z-Q, Fu Z, Miao J, Huang L, Chai S, et al. Spin-orbit coupled degenerate Fermi gases. Phys Rev Lett 2012;109(9):095301.
[6] Lin Y-J, Jiménez-García K, Spielman IB. Spin–orbit-coupled Bose–Einstein condensates. Nature 2011;471(7336):83–6.
[7] Stamper-Kurn DM, Ueda M. Spinor Bose gases: symmetries, magnetism, and quantum dynamics. Rev Mod Phys 2013;85:1191–244. doi:10.1103/RevModPhys.85.1191.
[8] Kawaguchi Y, Ueda M. Spinor Bose–Einstein condensates. Phys Rep 2012;520:253–381. doi:10.1016/j.physrep.2012.07.005.
[9] Widera A, Gerbier F, Fölling S, Gericke T, Mandel O, Bloch I. Precision measurement of spin-dependent interaction strengths for spin-1 and spin-2 ^{87}Rb atoms. New J Phys 2006;8:152. doi:10.1088/1367-2630/8/8/152.
[10] Kronjäger J, Becker C, Navez P, Bongs K, Sengstock K. Magnetically tuned spin dynamics resonance. Phys Rev Lett 2006;97:110404. doi:10.1103/PhysRevLett.97.110404.
[11] Schmaljohann H, Erhard M, Kronjäger J, Kottke M, van Staa S, Cacciapuoti L, Arlt JJ, Bongs K, Sengstock K. Dynamics of $F = 2$ spinor Bose–Einstein condensates. Phys Rev Lett 2004;92:040402. doi:10.1103/PhysRevLett.92.040402.
[12] Kuwamoto T, Araki K, Eno T, Hirano T. Magnetic field dependence of the dynamics of ^{87}Rb spin-2 Bose–Einstein condensates. Phys Rev A 2004;69:063604. doi:10.1103/PhysRevA.69.063604.
[13] Black AT, Gomez E, Turner LD, Jung S, Lett PD. Spinor dynamics in an antiferromagnetic spin-1 condensate. Phys Rev Lett 2007;99:070403. doi:10.1103/PhysRevLett.99.070403.
[14] Liu Y, Jung S, Maxwell SE, Turner LD, Tiesinga E, Lett PD. Quantum phase transitions and continuous observation of spinor dynamics in an antiferromagnetic condensate. Phys Rev Lett 2009;102:125301. doi:10.1103/PhysRevLett.102.125301.
[15] Bookjans EM, Vinit A, Raman C. Quantum phase transition in an antiferromagnetic spinor Bose–Einstein condensate. Phys Rev Lett 2011;107:195306. doi:10.1103/PhysRevLett.107.195306.
[16] Jacob D, Shao L, Corre V, Zibold T, De Sarlo L, Mimoun E, et al. Phase diagram of spin-1 antiferromagnetic Bose–Einstein condensates. Phys Rev A 2012;86:061601. doi:10.1103/PhysRevA.86.061601.
[17] Zhao L, Jiang J, Tang T, Webb M, Liu Y. Dynamics in spinor condensates tuned by a microwave dressing field. Phys Rev A 2014;89:023608. doi:10.1103/PhysRevA.89.023608.
[18] Chang M-S, Qin Q, Zhang W, You L, Chapman MS. Coherent spinor dynamics in a spin-1 Bose condensate. Nat Phys 2005;1:111–16. doi:10.1038/nphys153.
[19] Theis M, Thalhammer G, Winkler K, Hellwig M, Ruff G, Grimm R, et al. Tuning the scattering length with an optically induced Feshbach resonance. Phys Rev Lett 2004;93(12):123001.
[20] Blatt S, Nicholson T, Bloom B, Williams J, Thomsen J, Julienne P, et al. Measurement of optical Feshbach resonances in an ideal gas. Phys Rev Lett 2011;107(7):073202.
[21] Hamley CD, Bookjans EM, Behin-Aein G, Ahmadi P, Chapman MS. Photoassociation spectroscopy of a spin-1 Bose–Einstein condensate. Phys Rev A 2009;79:023401. doi:10.1103/PhysRevA.79.023401.
[22] Gerton JM, Frew BJ, Hulet RG. Photoassociative frequency shift in a quantum degenerate gas. Phys Rev A 2001;64:053410. doi:10.1103/PhysRevA.64.053410.
[23] Bohn JL, Julienne PS. Semianalytic theory of laser-assisted resonant cold collisions. Phys Rev A 1999;60:414–25. doi:10.1103/PhysRevA.60.414.
[24] Ospelkaus S, Ni KK, Wang D, de Miranda MHG, Neyenhuis B, Quéméner G, Julienne PS, Bohn JL, Jin DS, Ye J. Quantum-state controlled chemical reaction of ultracold potassium-rubidium molecules. Science 2010;327:853–7. doi:10.1126/science.1184121.
[25] Prodan ID, Pichler M, Junker M, Hulet RG, Bohn JL. Intensity dependence of photoassociation in a quantum degenerate atomic gas. Phys Rev Lett 2003;91:080402. doi:10.1103/PhysRevLett.91.080402.
[26] Junker M, Dries D, Welford C, Hitchcock J, Chen YP, Hulet RG. Photoassociation of a Bose–Einstein condensate near a Feshbach resonance. Phys Rev Lett 2008;101:060406. doi:10.1103/PhysRevLett.101.060406.
[27] Simoni A, Julienne PS, Tiesinga E, Williams CJ. Intensity effects in ultracold photoassociation line shapes. Phys Rev A 2002;66(6):063406.
[28] Wu J, Ji Z, Zhang Y, Wang L, Zhao Y, Ma J, Xiao L, Jia S. High sensitive determination of laser-induced frequency shifts of ultracold cesium molecules. Opt Lett 2011;36:2038–40. doi:10.1364/OL.36.002038.
[29] Li Y, Feng G, Liu W, Wu J, Ma J, Xiao L, et al. Control of laser-induced frequency shift in ultracold cesium molecules by an external magnetic field. Opt Lett 2015. doi:10.1364/OL.40.002241.
[30] Liu W, Wang X, Wu J, Su X, Wang S, Sovkov VB, et al. Experimental observation and determination of the laser-induced frequency shift of hyperfine levels of ultracold polar molecules. Phys Rev A 2017;96:022504. doi:10.1103/PhysRevA.96.022504.
[31] Danzl JG, Mark MJ, Haller E, Gustavsson M, Hart R, Aldegunde J, et al. An ultracold high-density sample of rovibronic ground-state molecules in an optical lattice. Nat Phys 2010;6:265–70. doi:10.1038/nphys1533.
[32] Kim J, Moal S, Portier M, Dugué J, Leduc M, Cohen-Tannoudji C. Frequency shifts of photoassociative spectra of ultracold metastable helium atoms: a new measurement of the *s*-wave scattering length. Europhys Lett 2005;72:548–54. doi:10.1209/epl/i2005-10275-y.
[33] Hopkins S, Butler K, Guttridge A, Kemp S, Freytag R, Hinds E, et al. A versatile dual-species Zeeman slower for caesium and ytterbium. Rev Sci Instrum 2016;87(4):043109.
[34] Raab E, Prentiss M, Cable A, Chu S, Pritchard DE. Trapping of neutral sodium atoms with radiation pressure. Phys Rev Lett 1987;59(23):2631.
[35] Chu S, Hollberg L, Bjorkholm JE, Cable A, Ashkin A. Three-dimensional viscous confinement and cooling of atoms by resonance radiation pressure. Phys Rev Lett 1985;55(1):48.
[36] Jiang J, Zhao L, Webb M, Jiang N, Yang H, Liu Y. Simple and efficient all-optical production of spinor condensates. Phys Rev A 2013;88:033620. doi:10.1103/PhysRevA.88.033620.
[37] Chang M-S, Hamley CD, Barrett MD, Sauer JA, Fortier KM, Zhang W, You L, Chapman MS. Observation of spinor dynamics in optically trapped ^{87}Rb Bose–Einstein condensates. Phys Rev Lett 2004;92:140403. doi:10.1103/PhysRevLett.92.140403.
[38] Li Y, Wang X, Wu J, Feng G, Liu W, Sovkov V, Ma J, Deb B, Xiao L, Jia S. The effects of a Feshbach resonance on spectral shifts in photoasociation of Cs atoms. Phys Chem Chem Phys 2021;23:641–6. doi:10.1039/D0CP04840B.
[39] Deb B, Agarwal GS. Feshbach resonance-induced Fano interference in photoassociation. J Phys B 2009;42:215203. doi:10.1088/0953-4075/42/21/215203.
[40] Deb B. Magneto-optical Feshbach resonance: controlling cold collision with quantum interference. J Phys B 2010;43:085208. doi:10.1088/0953-4075/43/8/085208.
[41] Feshbach H. Unified theory of nuclear reactions. Ann Phys 1958;5:357–90. doi:10.1016/0003-4916(58)90007-1.
[42] Feshbach H. A unified theory of nuclear reactions. II. Ann Phys 1962;19:287–313. doi:10.1016/0003-4916(62)90221-X.
[43] Feshbach H. The unified theory of nuclear reactions. Ann Phys 1967;43:410–20. doi:10.1016/0003-4916(67)90163-7.
[44] Fano U. Effects of configuration interaction on intensities and phase shifts. Phys Rev 1961;124:1866–78. doi:10.1103/PhysRev.124.1866.
[45] Fano U, Cooper JW. Line profiles in the far-UV absorption spectra of the rare gases. Phys Rev 1965;137:A1364–79. doi:10.1103/PhysRev.137.A1364.